



TECHNICAL ARTICLE

Effect of Niobium on Microstructure and Mechanical Properties of Ductile Iron with High Strength and Ductility

Haojie Wang, Yicheng Feng, Wenyong Jiang, Changliang Wang, Erjun Guo, Yuanke Fu, and Sicong Zhao

Submitted: 10 October 2022 / Revised: 22 November 2022 / Accepted: 20 December 2022 / Published online: 6 March 2023

The effect of niobium (Nb) on the microstructure and mechanical properties of ductile iron was investigated by metallographic analysis and mechanical tests. The analysis of precipitates by scanning electron microscopy (SEM) and energy-dispersive spectroscopy (EDS) reveals that the precipitated phase with a size less than 5 μm is composed of Nb, Mo and C. The phase diagram obtained by thermodynamic calculation and cooling curve analysis shows the precipitation of NbC during the solidification. The microstructure analysis indicates that the addition of Nb deteriorates the morphology of graphite and promotes the formation of pearlite. The mechanical properties analysis shows that the addition of Nb in ductile iron increases the hardness and strength, but decreases the elongation and impact toughness. The optimum value of ultimate tensile strength and yield strength is achieved at the Nb content of 0.14%. With the Nb addition of 0.14%, the hardness, ultimate tensile strength, yield strength, elongation and impact toughness are 182.3 HBW, 530.6 MPa, 405.2 MPa, 16.6% and 91.5 J/cm², respectively.

Keywords ductile iron, microalloying, microstructure, mechanical properties, niobium

1. Introduction

Ductile iron is a kind of cast iron with nodular graphite by nodularizer addition, and its strength and toughness are higher than that of gray cast iron with lamellar graphite. The applications of ductile iron range from mundane (cookwares, manhole covers) to advanced equipment (nuclear storage casks, windmills) due to the excellent mechanical properties and low cost. So the production of ductile iron is more and more, and the global production of ductile iron in 2019 was 23.66 million tons, accounting for 21.7% of the total output of metal castings (Ref 1). However, the requirements for mechanical properties of ductile iron are demanding, such as 100-ton class nuclear storage casks and windmills (hubs and rotor housings) (Ref 2, 3). Many researchers tried to improve the mechanical properties of ductile iron by the method of alloying and heat treatment. However, heat treatment of such large castings is difficult and

costly, and the best approach to achieve the specification in the as-cast condition is alloying. The general alloying elements, such as Cu and Ni, can improve the strength of ductile iron, but decrease the impact toughness and elongation significantly (Ref 4, 5). Therefore, the ductile iron alloyed by general elements cannot meet the requirements for mechanical properties. As a microalloying element, small amounts of Nb (0.05–0.14 wt.%) in carbon steel can reach an ultimate tensile strength of 450 MPa and an elongation of 30% by the effect of dispersion strengthening, solid solution strengthening and grain refinement strengthening (Ref 6). It can be inferred that the ductile iron alloyed by Nb can obtain a comprehensive mechanical property.

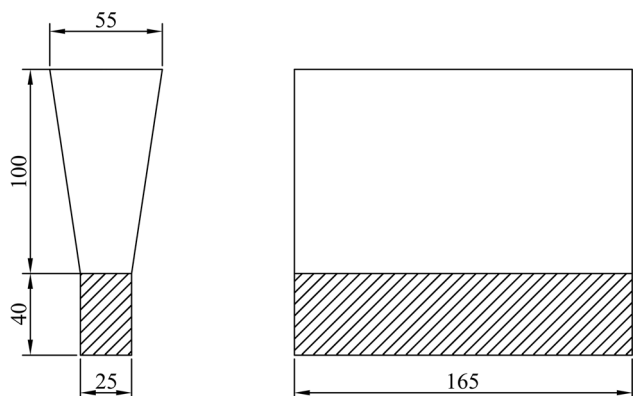
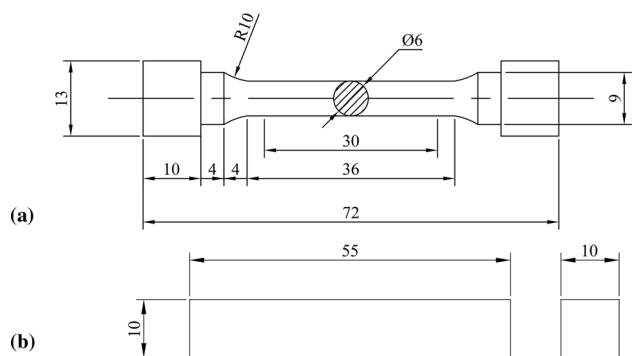
Nb is precipitated in the formation of polygonal NbC particles with a microsize and a microhardness of 1600–1800 HV (Ref 7). Yan (Ref 8) found that the addition of 0.69% Nb deteriorated the morphology of graphite, whose nodularity and counts of graphite decreased by 8.7 and 40%, respectively. Chen (Ref 9) indicated that the ultimate tensile strength of ductile iron was increased 75 MPa for the Nb content up to 0.08% due to the promotion of pearlite formation and the refinement of pearlite spacing by Nb. Souza (Ref 10) found that the impact toughness of ductile iron was reduced by nearly 50% with a content of 0.85% Nb since the content of graphite and ferrite was decreased. Chen (Ref 11) pointed out that the optimum wear resistance of austempered ductile iron was achieved in the content of 0.55% Nb, followed by an abrupt decrease with more Nb contents due to the reduction of bainite.

To determine the mechanism of Nb in the cast iron, some researchers (Ref 11–13) investigated the precipitation of NbC during the solidification. Thermodynamic calculation by Zhou (Ref 12) revealed that the temperature of the NbC precipitation was higher than eutectic reaction when the Nb content above 0.29% in gray cast iron, resulting in the precipitation of NbC from liquid phase. The graphite and eutectic cell were refined by the Nb addition (up to 0.85%) in gray cast iron, because the NbC acted as heterogeneous nucleation cores and can hinder

Haojie Wang, Wenyong Jiang, Changliang Wang, Erjun Guo, and Yuanke Fu, School of Materials Science and Chemical Engineering, Harbin University of Science and Technology, Harbin 150040, China; and Yicheng Feng and Sicong Zhao, School of Materials Science and Chemical Engineering, Harbin University of Science and Technology, Harbin 150040, China; and Key Laboratory of Advanced Manufacturing and Intelligent Technology, Ministry of Education, Harbin University of Science and Technology, Harbin 150080, China. Contact e-mail: fyc7806067@163.com.

Table 1 Chemical composition of investigated ductile iron (wt.%)

Samples	C	Si	Nb	Mo	Al	P	S	Mg	Ce
1	3.62	2.67	0	0.30	0.19	0.03	0.00033	0.076	0.057
2	3.54	2.64	0.05	0.31	0.18	0.02	0.00028	0.068	0.054
3	3.57	2.65	0.10	0.30	0.17	0.03	0.00031	0.065	0.058
4	3.58	2.63	0.14	0.32	0.18	0.03	0.00035	0.072	0.064
5	3.61	2.72	0.19	0.30	0.18	0.02	0.00030	0.070	0.060

**Fig. 1** Diagram of the standard Y-block (mm)**Fig. 2** Diagram of the mechanical specimens (mm). (a) Tensile specimen; (b) impact specimen

the C diffusion. Chen (Ref 11) compared the Nb solubility in austenite and liquid phase of ductile iron at the eutectic temperature and found that with the Nb addition below 0.07%, in 0.07-0.17% and above 0.17% in ductile iron, the NbC will precipitate from austenite, during the eutectic reaction and from liquid phase, respectively. The results showed that the Nb addition of 0.21%-1.06% in ductile iron decreased the nodularity and nodule counts of graphite due to the hindrance of C diffusion and consumption of C. Ahmed (Ref 13) calculated the phase diagram of Nb in austempered ductile iron by Thermo-Calc software, which showed that the NbC will precipitate during the eutectic reaction with the Nb addition of 0.01-0.11%. Their results showed that with increasing the Nb content to 0.10%, the nodule counts increased, while the nodularity decreased slightly. The nano-sized NbC can also act as nucleation sites for graphite and ferrite needles, thus accelerating the ausferrite formation.

Table 2 Interaction coefficient of elements in liquid iron at 1873 K (Ref 20)

	C	Si	Nb	Mo	Al
e_C^j	0.14	0.08	-0.06	-0.0083	0.043
e_{Nb}^j	-0.49	0	0	0	0

Both the effect and mechanism of Nb in ductile iron were investigated by some researchers, but this studies mainly concentrated in low Nb content (< 0.10%) or high Nb content (> 0.20%) which cannot include the whole eutectic reaction. To analyze the effect of Nb in solidification, it is necessary to study the ductile iron with 0-0.20% Nb. The main purpose of this paper is to explore the mechanism of Nb in the solidification of ductile iron by comparing the temperature of NbC precipitation and eutectic reaction, which are obtained by thermodynamic calculation and cooling curve analysis, respectively. Based on the mechanism, the influence of Nb on microstructure and mechanical properties is explained.

2. Experimental Procedures

2.1 Specimen Preparation

The nominal chemical composition of ductile iron contains 3.6 C, 2.7% Si, Nb (0, 0.05, 0.10, 0.15, 0.20%), 0.30 Mo and 0.20% Al, the addition of Mo can improve the precipitation strengthening effect by forming (Nb, Mo)C with Nb (Ref 14), and the addition of Al can improve the nucleation rate and the graphite content (Ref 15). The results of tested chemical composition are given in Table 1. The raw materials included pig iron, carbon steel, ferro-molybdenum (56% Mo), ferro-niobium (60% Nb), nodularizer (8.2 Mg, 2.5% RE, 4-10 mm), ferro-silicon (72% Si) primary inoculant (4-10 mm) and ferro-silicon secondary inoculant (0.5-1 mm).

Pig iron, ferro-niobium, ferro-molybdenum and carbon steel were melted and homogenized at 1500-1550 °C in a medium-frequency induction furnace with a capacity of 50 kg. The nodularization treatment was achieved by the “sandwich” method which placed the nodularizer, primary inoculant covered with iron filings in the bottom of preheated ladle, and the molten iron was poured into the ladle. After the slag was skimmed from the surface of nodularized molten iron, the secondary inoculant was added into molten iron. The molten iron was poured into the sand mold to obtain the standard Y-block specimen according to ISO 1083:2018 standard as shown

Table 3 Precipitation temperature of NbC in ductile iron with different Nb contents

Nb content, %	0.05	0.10	0.14	0.19
Precipitation temperature of NbC, K	1304.5	1374.7	1411.3	1446.0

in Fig. 1, and the shaded part was used for microstructural analysis and mechanical properties testing. The time from tapping to pouring was controlled within 8 min to obtain a high pouring temperature.

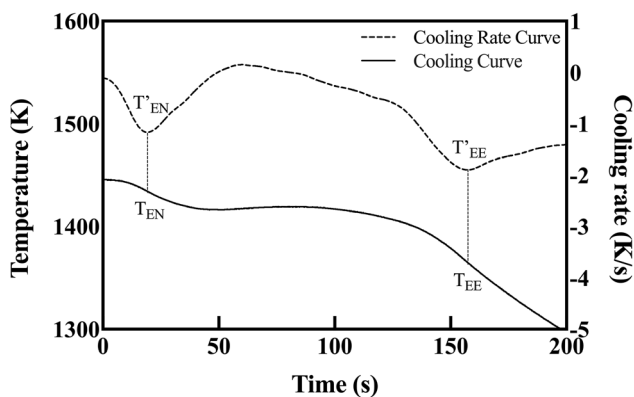


Fig. 3 Cooling curve and cooling rate curve of ductile iron with the Nb content of 0.05%

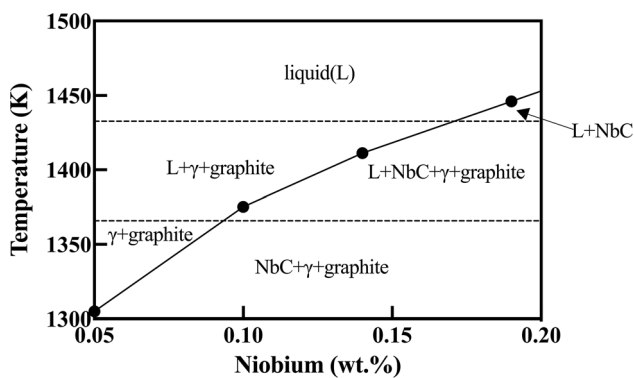


Fig. 4 Phase diagram of Nb in ductile iron

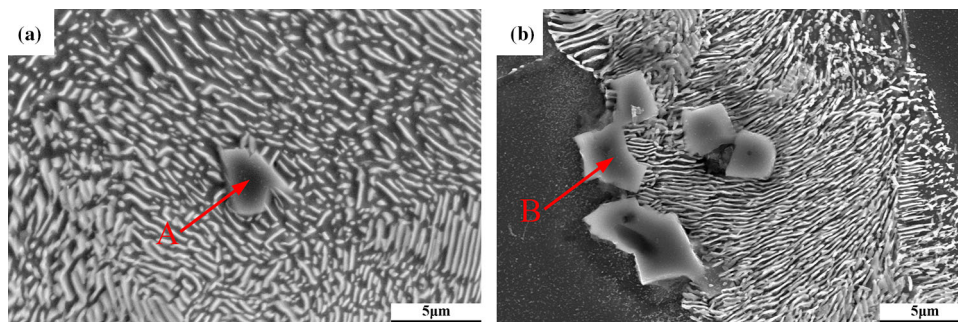


Fig. 5 Precipitated phase in ductile iron with different Nb contents. (a) 0.05%; (b) 0.19%

2.2 Microstructural Analysis

Metallographic specimens were grinded followed by polishing and etching with 4% Nital. The microstructure of the ductile iron was observed by optical microscopy (OLYMPUS-GX71) and scanning electron microscopy (Thermo Scientific TM Apreo C).

The graphite morphology was analyzed by image analysis software following the ISO 945-4:2019 standard. The graphite roundness(r) was calculated by the following equation:

$$r = \frac{A}{A_m} = \frac{4A}{\pi l_m^2} \quad (\text{Eq 1})$$

where l_m is the maximum Féret diameter of the graphite particle, A is the area of graphite particle and A_m is the area of circle diameter l_m .

The nodularity (P) of graphite particles was calculated by the following formula:

$$P = \frac{A_0}{A_{\text{all}}} \quad (\text{Eq 2})$$

where A_0 is the total area of graphite particles with $r \geq 0.6$ and A_{all} is the total area of all graphite particles. Graphite particles with l_m less than 10 μm should be excluded from the evaluation.

The lamellar spacing of pearlite was measured by the method provided by Voort (Ref 16). Test circle was randomly applied on the pearlite, and the number of intersections of cementite with test circle was counted. The lamellar spacing of pearlite was calculated by the following formula:

$$S = \frac{\pi d}{nM} \quad (\text{Eq 3})$$

where S is the random lamellar spacing of pearlite, d is the diameter of test circle, n is the number of intersections of cementite with test circle and M is the magnification. At least 50 circles were drawn on each specimen to obtain the average pearlite lamellar spacing.

2.3 Solidification Analysis

To obtain the cooling curves of ductile iron, a K-type thermocouple sheathed by a ceramic tube was set in the central point of a sand cup with dimensions of $\Phi 30 \text{ mm} \times 45 \text{ mm}$ and with a thickness of 5 mm. The temperature data were recorded per 0.1 s by the data acquisition system to obtain the cooling

curves, which were derived in Origin software to identify the critical temperatures.

2.4 Mechanical Testing

The Brinell hardness of ductile iron was tested by a 310HBS-3000 Brinell durometer (load of 750 kg and spherical indenter with diameter 5 mm) according to ISO 6506-1:2014 standard. The tensile specimens with a diameter of 6 mm and a

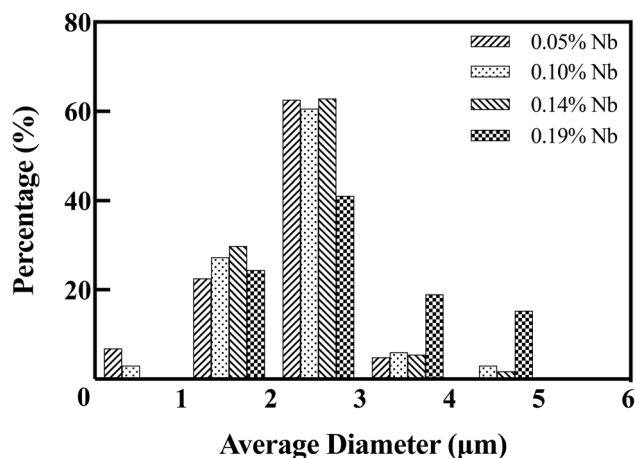


Fig. 6 Precipitated phase size distributions of ductile iron with different Nb contents

Table 4 Atomic percentage of elements corresponding to point A and point B in Fig. 5, at. %

Point	C	Fe	Nb	Mo
A	64.10	1.86	26.09	7.95
B	68.02	2.42	27.51	2.05

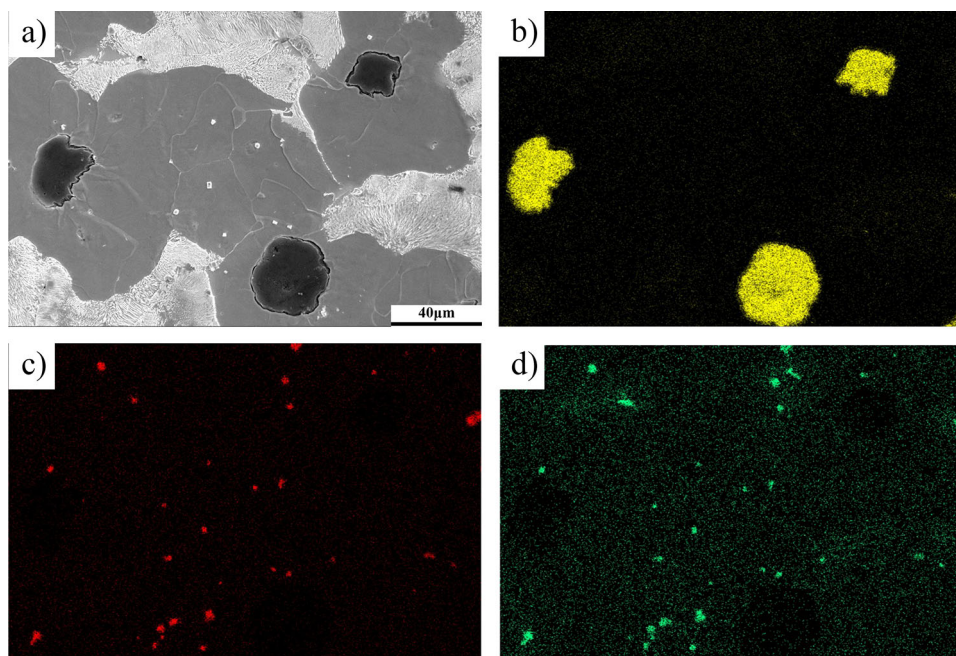


Fig. 7 EDS map of ductile iron with the Nb content of 0.19%. (a) Microstructure; (b) C; (c) Nb; (d) Mo

gauge length of 30 mm were tested by XYB305C universal mechanical testing machine according to ISO 6892-1:2019 standard. The non-notched impact specimens were tested by the JBN-300B impact testing machine according to ISO 148-1:2016 standard (Fig. 2).

3. Results and Discussion

3.1 The Mechanism of Nb in Solidification

The melting point of ferro-niobium (60% Nb) is about 1500-1510 °C (Ref 17), which is lower than the temperature of liquid iron, so ferro-niobium can be melted in liquid iron to form solute Nb. As the temperature of liquid iron decreases, the solute Nb will combine with solute C to form NbC with a face-centered cubic structure (Ref 18). To determine the influence of Nb contents on the precipitation temperature of NbC in ductile iron, the thermodynamic calculation is carried out according to the method of Zhou (Ref 12).

The formation of NbC is shown as follows:



Its standard Gibbs free energy can be calculated (Ref 12) as:

$$\Delta G^\ominus = -182490 + 96.99T \quad (\text{Eq 5})$$

Gibbs free energy at atmospheric pressure can be expressed (Ref 19) as:

$$\begin{aligned} \Delta G &= \Delta G^\ominus + RT \ln \left(\prod \alpha_B \right) \\ &= \Delta G^\ominus - RT \ln \left(\alpha_C \cdot \alpha_{Nb} \right) \\ &= \Delta G^\ominus - RT \ln \left(f_c \cdot w_c \% \cdot f_{Nb} \cdot w_{Nb} \% \right) \end{aligned} \quad (\text{Eq 6})$$

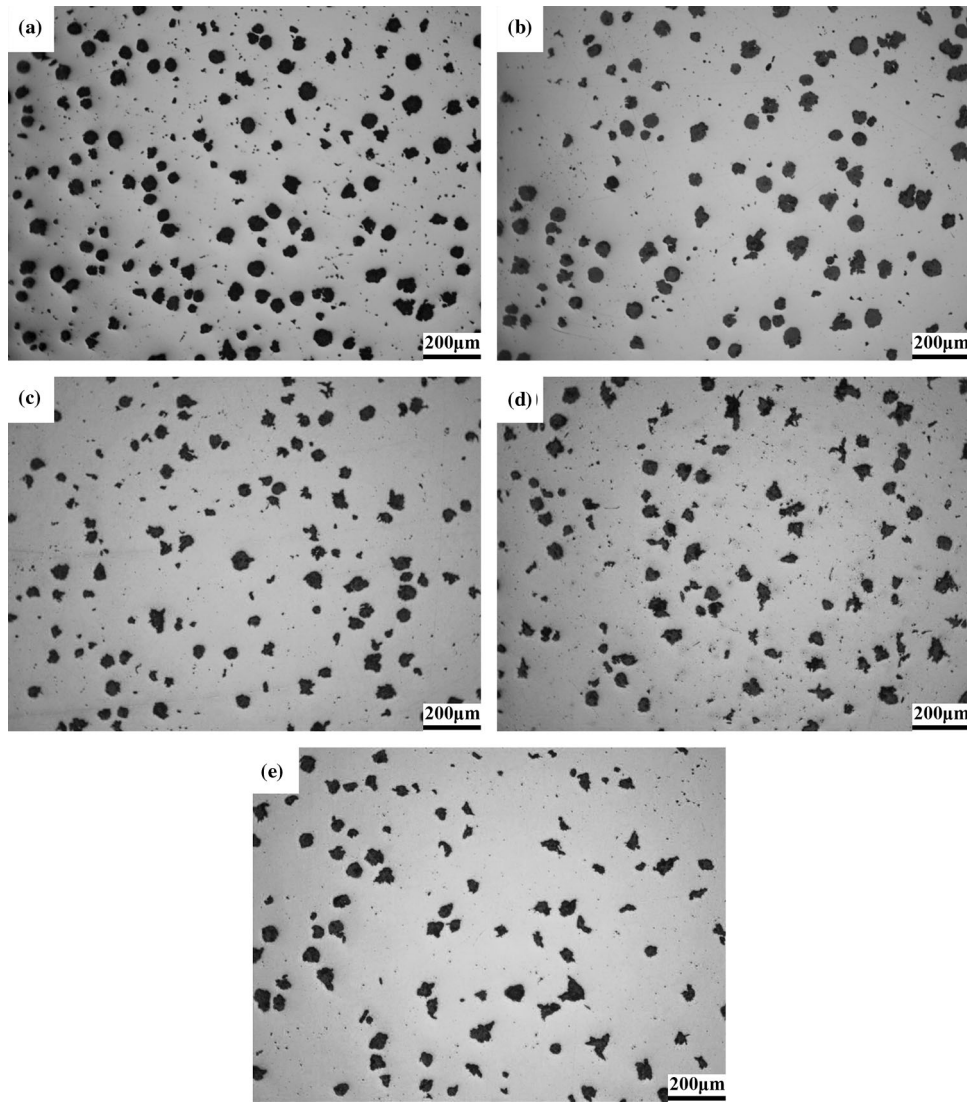


Fig. 8 Graphite morphology of ductile iron with different Nb contents. (a) 0%; (b) 0.05%; (c) 0.10%; (d) 0.14%; (e) 0.19%

Table 5 Graphite morphology statistics of ductile iron with different Nb contents

Nb content, %	Nodularity, %	Graphite diameter, μm	Graphite particle, counts/ mm^2	Graphite content, %
0	80	50	142	10.8
0.05	77	55	133	10.2
0.10	69	46	115	7.2
0.14	61	52	98	6.6
0.19	57	48	99	5.4

where f_c and f_{Nb} are the activity coefficients and can be calculated using Eq 7 and 8, respectively (Ref 20). R is the molar gas constant, and its value is 8.314 J/(mol·K).

$$\lg f_c = e_C^C w_C\% + e_C^{\text{Si}} w_{\text{Si}}\% + e_C^{\text{Nb}} w_{\text{Nb}}\% + e_C^{\text{MO}} w_{\text{MO}}\% + e_C^{\text{Al}} w_{\text{Al}}\% \quad (\text{Eq 7})$$

$$\lg f_{\text{Nb}} = e_{\text{Nb}}^C w_C\% + e_{\text{Nb}}^{\text{Si}} w_{\text{Si}}\% + e_{\text{Nb}}^{\text{Nb}} w_{\text{Nb}}\% + e_{\text{Nb}}^{\text{MO}} w_{\text{MO}}\% + e_{\text{Nb}}^{\text{Al}} w_{\text{Al}}\% \quad (\text{Eq 8})$$

where e_C^C , e_C^{Si} are the interaction coefficients of different elements in the liquid iron, and $w_C\%$ and $w_{\text{Nb}}\%$ are the contents of different elements.

The thermodynamic data of e_i^j in 1873 K are shown in Table 2. The e_i^j in T can be calculated using Eq 9 by regarding the liquid iron as a regular solution.

$$e_{i(T)}^j = \frac{1879}{T} e_{i(1873\text{K})}^j \quad (\text{Eq 9})$$

Gibbs free energy at atmospheric pressure can be obtained as follows by substituting the thermodynamic data of Table 2 into Eq 6.

$$\Delta G = -145275.28 + 86.34T + 2151.37w_{\text{Nb}}\% - 8.314T \ln(w_{\text{Nb}}\%) \quad (\text{Eq 10})$$

When $\Delta G=0$,

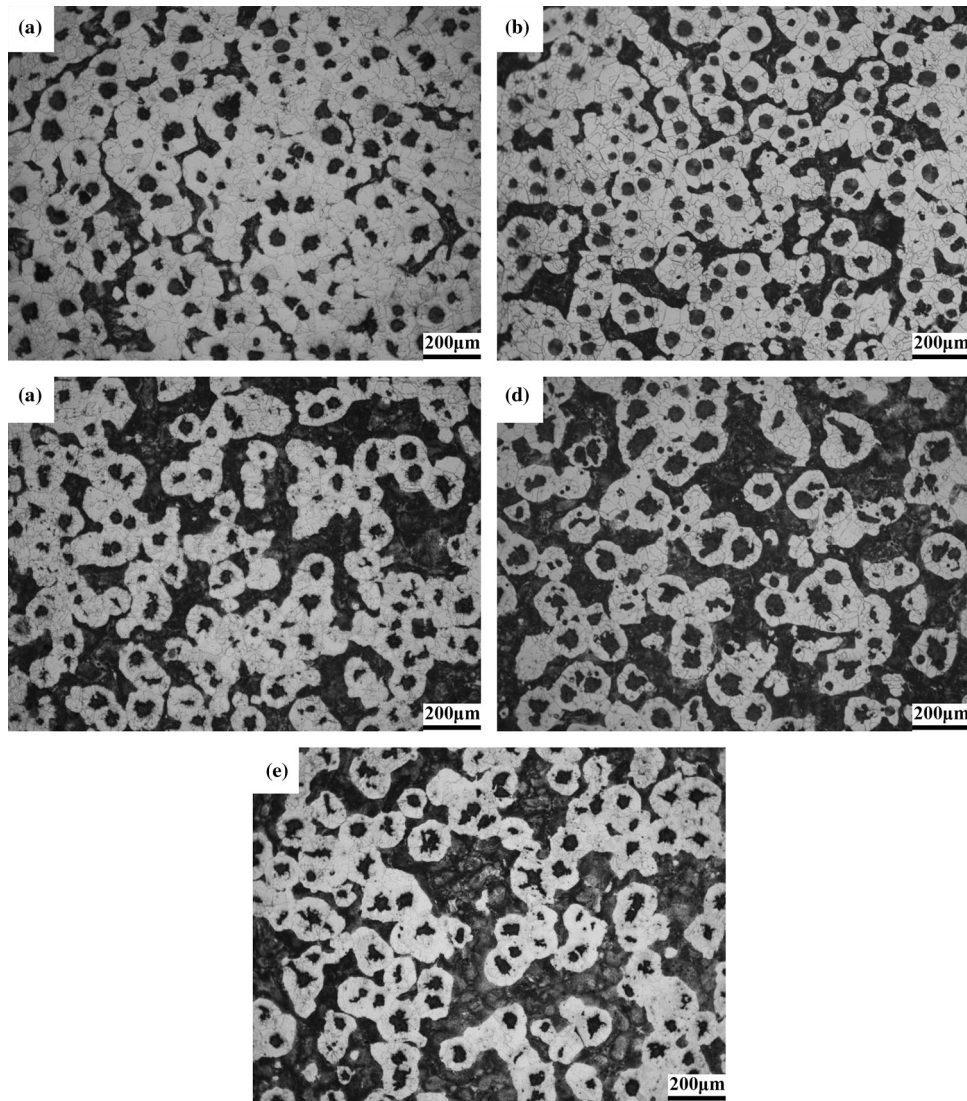


Fig. 9 Matrix microstructure of ductile iron with different Nb contents. (a) 0%; (b) 0.05%; (c) 0.10%; (d) 0.14%; (e) 0.19%

$$T = \frac{-145275.28 + 2151.37w_{\text{Nb}}\%}{86.34 - 8.314T \ln(w_{\text{Nb}})\%} \quad (\text{Eq 11})$$

The precipitation temperature of NbC can be obtained according to Eq 11, and the specific values are shown in Table 3.

The cooling curve of ductile iron was obtained to determine the temperature relationship between NbC precipitation and eutectic reaction. Figure 3 shows the cooling curve and its first derivative (cooling rate curve). T_{EN} and T_{EE} are the local minimum points on the cooling rate curve, corresponding to the eutectic start temperature (T_{EN}) and eutectic end temperature (T_{EE}), respectively (Ref 21). The analysis shows that the T_{EN} and T_{EE} are 1432.8 and 1365.9 K with 0.05% Nb addition in ductile iron.

The phase diagram of Nb in ductile iron (primary austenite is not included) as shown in Fig. 4 can be obtained by the temperature date of NbC precipitation and eutectic reaction. It can be seen from the phase diagram that ductile iron with a Nb content of 0.05% cannot precipitate NbC during the solidification, and is only affected by the drag of solute Nb. Solute

drag refers to the motion of boundaries and is retarded due to the heterogeneous distribution of Nb on both sides of the boundaries (Ref 22). The ductile iron with a Nb content of 0.10-0.14% will precipitate NbC during the eutectic reaction and is affected by the Zener pinning of NbC and the drag of solute Nb. Zener pinning means that the migration velocity of boundaries is decreased due to the surface tension of NbC in the boundaries (Ref 23). The ductile iron alloyed by 0.19% Nb will precipitate NbC in liquid phase. The minimum lattice misfit between the NbC and graphite is 7.2% (Ref 24), so NbC can be considered as a potent graphite nucleation site (Ref 25). Therefore, ductile iron with a Nb addition of 0.19% is influenced by the comprehensive effect of Zener pinning and nucleation sites.

3.2 Precipitated Phase

Figure 5 shows the morphology of the precipitated phase in ductile iron with a Nb content of 0.05 and 0.19%. It can be seen that the precipitated phases are micro-sized due to the coarsening during the long time solidification at high temperature. The morphology of precipitates includes triangles, quadrilaterals

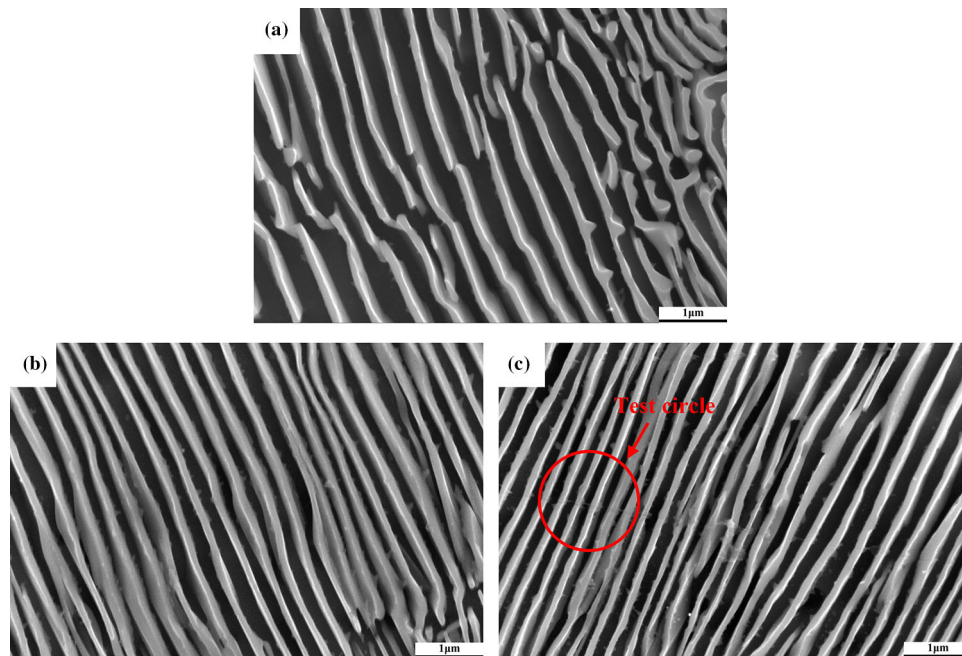


Fig. 10 Pearlite morphology of ductile iron with different Nb contents. (a) 0%; (b) 0.10%; (c) 0.19%

Table 6 Matrix microstructure statistics of ductile iron with different Nb contents

Nb content, %	Pearlite content, %	Pearlite lamellar spacing, μm	Ferrite diameter, μm
0	10.0	0.51	26.3
0.05	15.1	0.48	27.5
0.10	24.5	0.43	26.3
0.14	32.0	0.40	26.8
0.19	38.8	0.36	27.0

and polygons at a ratio of 1:17:13. The size distributions of precipitates are shown in Fig. 6. It can be seen that the size of all precipitates is less than $5 \mu\text{m}$, and most of the precipitates size is around $3 \mu\text{m}$. The size distribution of precipitates in ductile iron with a Nb content of 0.05-0.14% is coincident, but the proportion of large precipitates ($> 3 \mu\text{m}$) increases significantly at the Nb content of 0.19% because the precipitates formed in liquid phase have a higher growth rate.

To determine the chemical composition of precipitated phases, the EDS point was carried out in the arrow position of Fig. 5. The analysis of the EDS point in Table 4 shows that the precipitated phases are mainly composed of C, Fe, Nb and Mo. The Nb: Mo ratio of precipitated phases in ductile iron with the Nb content of 0.05 and 0.19% are closed to 3:1 and 13:1, respectively.

To obtain the distribution of precipitated phases, the EDS map of ductile iron alloyed by 0.19% Nb was carried out. Figure 7 shows that the highlight position of Nb and Mo is coincident. It can be also confirmed that the precipitated phases are heterogeneously distributed in both ferrite and pearlite.

3.3 Graphite Morphology

Figure 8 presents the graphite micrograph of unetched specimens. It is evident that the addition of Nb deteriorates the morphology of graphite. Table 5 shows that the Nb addition

decreases the nodularity, counts and content of graphite, while it has little influence on the graphite diameter. The variation of graphite morphology is significant in the Nb content of 0.05-0.14%, but negligible in other contents.

The Zener pinning of NbC is more effective than the darg of solute Nb in eutectic reaction, so the morphology of graphite is mainly affected by the NbC (Ref 22). The ductile iron with the Nb content of 0.05% cannot precipitate NbC during the eutectic reaction, resulting in little influence on the morphology of ductile iron. The ductile iron with 0.10-0.14% Nb addition precipitates NbC during the eutectic reaction, and the counts of NbC increase with the Nb content increasing. The austenite shell will be formed around the graphite when graphite contacts austenite (Ref 26), and the NbC around the austenite will decrease the closing rate of austenite shell by the effect of Zener pinning (Ref 27). The diffusion rate of C in liquid and austenite is different (Ref 28), so the reduction in the closing rate in austenite shell leads to the anisotropic growth of graphite to decrease nodularity. The addition of Nb in ductile iron decreases the graphite eutectic temperature and has little influence on the cementite eutectic temperature (Ref 29), resulting in the reduction in the graphite nucleation rate to decrease the graphite counts. The ductile iron with the Nb content of 0.19% will precipitate NbC before the eutectic reaction which can be the nucleation sites of graphite. With the Nb addition of 0.14-0.19%, the variation of graphite morphol-

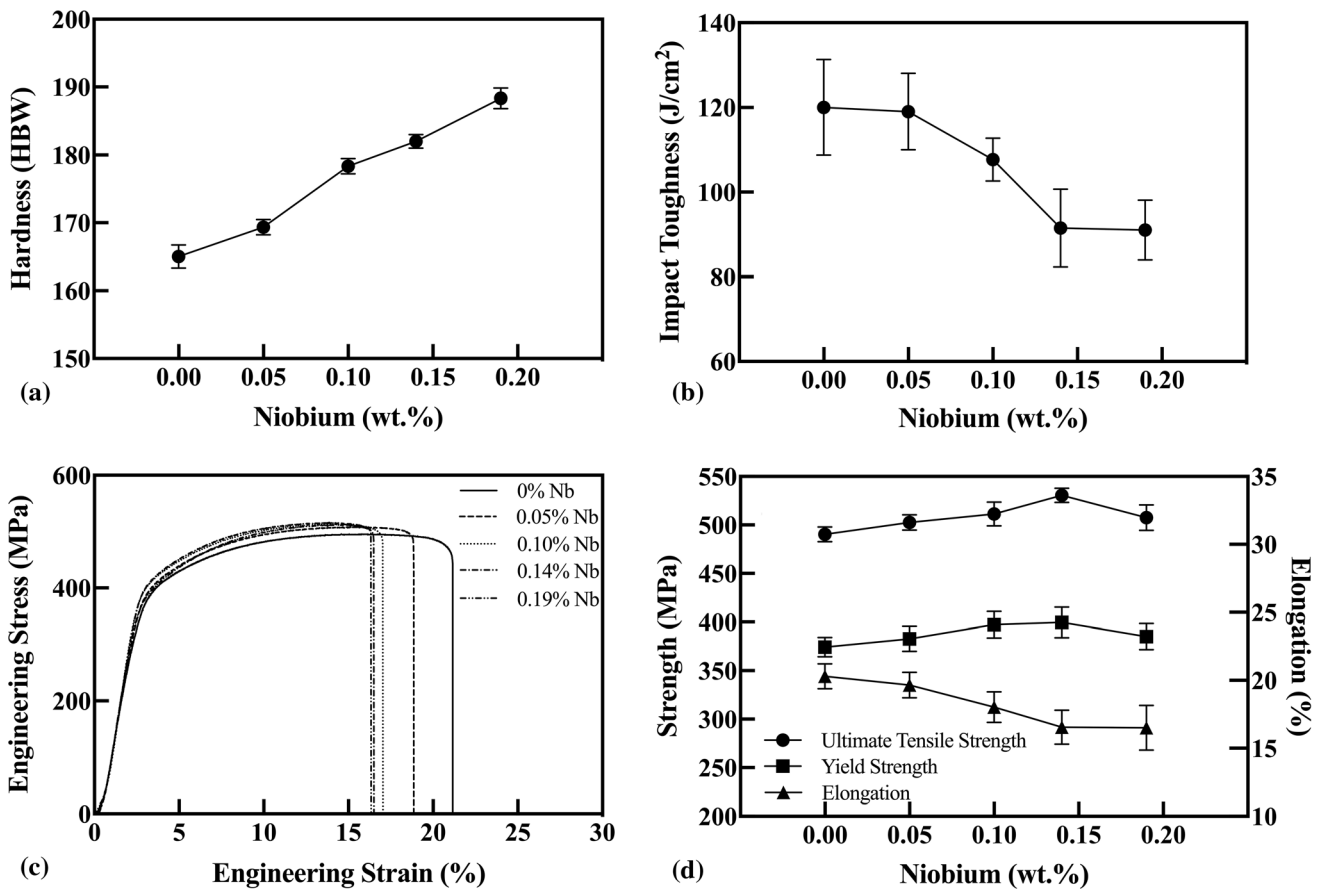


Fig. 11 Mechanical properties of ductile iron with different Nb contents. (a) hardness; (b) impact toughness; (c) engineering strain–stress curve; (d) strength and elongation

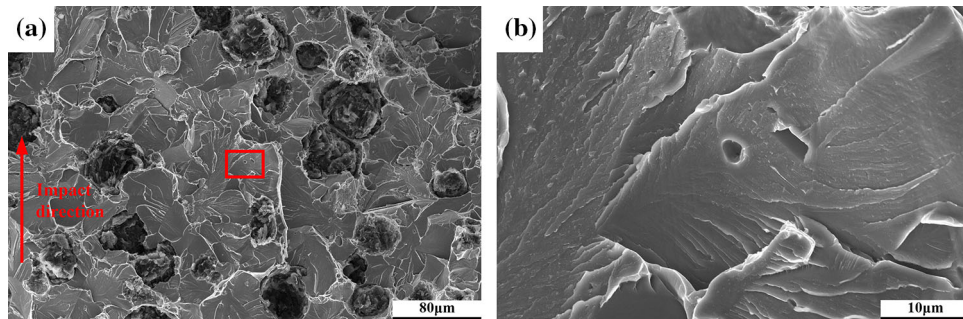


Fig. 12 Impact fracture surface of ductile iron with 0.10% Nb

ogy is negligible due to the comprehensive effect of Zener pinning and nucleation sites.

3.4 Matrix Microstructure

Figure 9 displays the optical micrographs of etched specimens. It is obvious that the ferrite around graphite becomes thinner and the pearlite content rises with the increase in the Nb content. Figure 10 shows the pearlite morphology of ductile iron with different Nb contents, and the test circle in Fig. 10(c) represents the region for measuring the lamellar spacing of pearlite. Table 6 shows the results of Nb effect in matrix microstructure, and it can be seen that the Nb addition increases

the pearlite content, decreases the pearlite lamellar spacing and has little effect in the ferrite diameter.

During the eutectoid reaction, austenite can transform into ferrite + graphite or ferrite + cementite (pearlite), and both the ferrite content and pearlite lamellar spacing are related to the carbon diffusion (Ref 30). On the one hand, the Nb addition in ductile iron can reduce the counts of graphite, increasing the distance of carbon diffusion. On the other hand, the Nb addition in ductile iron decreases the temperature of eutectoid reaction, which causes a reduction in carbon diffusion rate. Sun et al. concluded that the start temperature of eutectoid reaction was reduced 38 °C (cooling rate was 5 °C/s) with the addition of 0.04% Nb (Ref 6). Therefore, the addition of Nb in ductile can

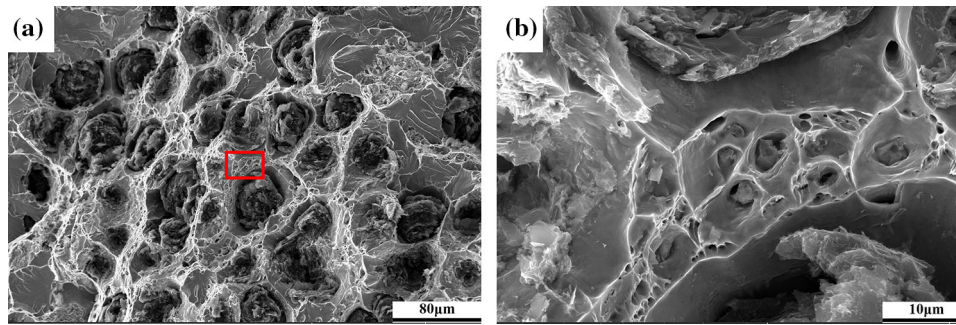


Fig. 13 Tensile fracture surfaces of ductile iron with 0.10% Nb contents

retard the diffusion of carbon to promote the pearlite formation and decrease the pearlite lamellar spacing.

3.5 Mechanical Properties

The mechanical properties are shown in Fig. 11, and it can be seen that the addition of Nb in ductile iron increases the hardness and strength, while it decreases the impact toughness and elongation. The addition of Nb increases the pearlite and NbC content, resulting in the decrease in the impact toughness and the increase in the hardness. The impact toughness is mainly related to the graphite, so the variation of impact toughness is similar to the graphite morphology which is significant in the Nb content of 0.05–0.14%, but negligible in other contents. The strength is improved by the precipitation strengthening of NbC, the increase in the pearlite content and the refinement of pearlite lamellar spacing. However, the addition of 0.20% Nb in ductile iron decreases the strength because of the NbC precipitate from liquid phase with a larger size, leading to the stress concentration.

To describe the detachment characteristics of NbC during the testing, the impact and tensile fracture surfaces were analyzed. The impact fracture surfaces in Fig. 12 consist of cleavage facets, and a micropore after NbC detachment in Fig. 12(b) is in a cleavage facet. Therefore, the NbC separates from matrix microstructure when the cracks propagate along the cleavage plane. The tensile fracture surfaces in Fig. 13 consist of dimples, and the NbC in Fig. 13(b) is distributed in the microvoids. It can be inferred that the cracks initiate at both NbC–matrix and graphite–matrix interfaces, so the size of NbC can affect the tensile properties due to the stress concentration.

4. Conclusions

In this paper, the effect of Nb content on the microstructure and mechanical properties of ductile iron with high strength and ductility was studied, and the following conclusions were drawn:

- (1) The phase diagram of Nb in ductile iron was drawn from the temperature date of NbC precipitation and eutectic reaction which were obtained by thermodynamic calculation and cooling curve analysis, respectively.
- (2) The precipitated phases with a size less than 5 μm were composed of Nb, Mo and C. The addition of Nb in ductile iron increased the content of pearlite and decreased

the nodularity, counts and content of graphite, while it had little effect in the diameter of graphite and ferrite.

- (3) The influence of Nb on the mechanical properties of ductile iron was significant. The comprehensive properties of ductile iron at the Nb addition of 0.14% with the hardness, yield strength, ultimate tensile strength, elongation and impact toughness were 182.3 HBW, 405.2 MPa, 530.6 MPa, 16.6% and 91.5 J/cm², respectively.

References

1. T.W.F. Organization, Census of World Casting Production: Total Casting Tons Dip in 2019, Jan (2021)
2. T. Arai, T. Saegusa, and R. Hueggenberg, Recent Development of Code Case on Use of Ductile Cast Iron for Transport and Storage Cask for Spent Nuclear Fuel, *ASME Press. Vessels Pip. Conf.*, 2008, **48302**, p 225–233
3. I. Ripsan, M. Chisamera, and S. Stan, Performance of Heavy Ductile Iron Castings for Windmills, *China Foundry*, 2010, **7**(2), p 163–170
4. H. Sazegaran, F. Teimoori, H. Rastegarian, and A.M. Naserian-Nik, Effects of Aluminum and Copper on the Graphite Morphology Microstructure, and Compressive Properties of Ductile Iron, *J. Min. Metall. B Metall.*, 2021, **57**(1), p 145–154
5. J. Ke, Q. Yingdong, Y. Junhua, and L. Rongde, Absorbed Energy Distribution of Ductile Ni-resist Alloyed Iron Under Instrumented Impact Load at Low Temperatures, *ISIJ Int.*, 2016, **56**(7), p 1285–1288
6. L. Sun, X. Liu, X. Xu, S. Lei, H. Li, and Q. Zhai, Review on Niobium Application in Microalloyed Steel, *J. Iron. Steel Res. Int.*, 2022, **29**, p 1513–1525
7. L.I. Rivera, V.A. Roca, C.F. Patiño, and C.M. Cruells, Microalloyed Niobium Influence on Ductile Ferrite Cast Irons, *Int. J. Cast Met. Res.*, 2003, **16**(1–3), p 65–70
8. Y. Yan, L. Chang, X. Chen, Q. Hua, and Q. Zhai, Effect of Niobium on the Morphology of Nodular Graphite in Ductile Iron, *Adv. Mater. Res.*, 2014, **852**, p 163–167
9. X. Chen, J. Xu, H. Hu, H. Mohrbacher, M. Kang, W. Zhang, A. Guo, and Q. Zhai, Effects of Niobium Addition on Microstructure and Tensile Behavior of As-Cast Ductile Iron, *Mater. Sci. Eng. A*, 2017, **688**, p 416–428
10. T.N.F. Souza, R. Nogueira, F.J.S. Franco, M.T.P. Aguilar, and P.R. Cetlin, Mechanical and Microstructural Characterization of Nodular Cast Iron (NCI) with Niobium Additions, *Mater. Res.*, 2014, **17**(5), p 1167–1172
11. X. Chen, L. Zhao, W. Zhang, H. Mohrbacher, W. Wang, A. Guo, and Q. Zhai, Effects of Niobium Alloying on Microstructure, Toughness and Wear Resistance of Austempered Ductile Iron, *Mater. Sci. Eng. A*, 2019, **760**, p 186–194
12. W. Zhou, H. Zhu, D. Zheng, H. Zheng, Q. Hua, and Q. Zhai, Niobium Alloying Effect in High Carbon Equivalent Grey Cast Iron, *China Foundry*, 2011, **8**, p 36–40

13. M. Ahmed, M. Soliman, M. Youssef, R. Baehr, and A. Nofal, Effect of Niobium on the Microstructure and Mechanical Properties of Alloyed Ductile Irons and Austempered Ductile Irons, *Metals*, 2021, **11**(5), p 703
14. W. Lee, S. Hong, C. Park, K. Kim, and S. Park, Influence of Mo on Precipitation Hardening in Hot Rolled HSLA Steels Containing Nb, *Scripta Mater.*, 2000, **43**(4), p 319–324
15. H. Sazegaran, F. Teimoori, H. Rastegarian, and A.M. Naserian-Nik, Effects of Aluminum and Copper on the Graphite Morphology Microstructure, and Compressive Properties of Ductile Iron, *J. Min. Metall. Sect. B Metall.*, 2021, **57**(1), p 145–154
16. G. Vander Voort and A. Roosz, Measurement of the Interlamellar Spacing of Pearlite, *Metallography*, 1984, **17**(1), p 1–17
17. E. Paul and L. Swartzendruber, The Fe-Nb (Iron-Niobium) System, *Bullet. Alloy Phase Diag.*, 1986, **7**(3), p 248–254
18. M.G.D. Cuppari and S.F. Santos, Physical Properties of the NbC Carbide, *Metals*, 2016, **6**(10), p 250
19. R.J. Silbey, R.A. Alberty, M.G. Bawendi, and G.A. Papadantonakis, *Physical Chemistry*, 4th ed., John Wiley & Sons, Hoboken, 2004, p 113–120
20. G.K. Sigworth and J.F. Elliott, The Thermodynamics of Liquid Dilute Iron Alloys, *Met. Sci.*, 1974, **8**(1), p 298–310
21. I. Stan, D. Anca, S. Stan, and I. Riposan, Solidification Pattern of Si-Alloyed Inoculated Ductile Cast Irons, Evaluated by Thermal Analysis, *Metals*, 2021, **11**(5), p 846
22. C.R. Hutchinson, H.S. Zurob, C.W. Sinclair, and Y.J. Brechet, The Comparative Effectiveness of Nb Solute and NbC Precipitates at Impeding Grain-Boundary Motion in Nb Steels, *Scripta Mater.*, 2008, **59**(6), p 635–637
23. M. Pa, M. Ferry and T. Chandra, Five Decades of the Zener Equation, *ISIJ Int.*, 1998, **38**(9), p 913–924
24. H. Mohrbacher, On the Metallurgical Effects of Niobium in Cast Iron Alloys, In: *WFO 2018 Conference* (Suzhou, China, 2018) p. 1–6
25. B.L. Bramfitt, The Effect of Carbide and Nitride Additions on the Heterogeneous Nucleation Behavior of Liquid Iron, *Metall. Trans.*, 1970, **1**(7), p 1987–1995
26. M. Zhu, L. Zhang, H. Zhao, and D.M. Stefanescu, Modeling of Microstructural Evolution during Divorced Eutectic Solidification of Spheroidal Graphite Irons, *Acta Mater.*, 2015, **84**, p 413–425
27. J. Wang, Z. Wang, S. Ren, R. Yan, K. Huang, and J. Guo, Effect of Ti Addition on Microstructure and Mechanical Properties of Ductile Iron, *J Jilin Univ (Eng Technol Edn)*, 2020, **50**(5), p 1653–1662. ((in Chinese))
28. J. Zhou and W. Schmitz, Formation of Austenite Shell around Spheroidal Graphite and Its Effect on Deterioration of Graphite, *Acta Metall. Sin.*, 1989, **25**(1), p 117–121
29. T. Kanno, Y. You, M. Morinaka, and H. Nakae, Effect of Alloying Elements on Graphite and Cementite Eutectic Temperature of Cast Iron, *J. Japan Foundry Eng. Soc.*, 1998, **70**(7), p 465–470. ((in Japanese))
30. H. Berns and W. Theisen, *Ferrous Materials: Steel and Cast Iron*, 1st ed. Springer, Berlin, Heidelberg, 2008, p 31–35

Publisher's Note Springer Nature remains neutral with regard to jurisdictional claims in published maps and institutional affiliations.

Springer Nature or its licensor (e.g. a society or other partner) holds exclusive rights to this article under a publishing agreement with the author(s) or other rightsholder(s); author self-archiving of the accepted manuscript version of this article is solely governed by the terms of such publishing agreement and applicable law.